Composite SnO_2-K_2S ETL for Energy Level Regulation and Electron Mobility Enhancement in Perovskite Solar Cells

Ruiyuan Hu [a, b*], Yongjun Li [a, c], Fan Zhang [a], Yuhui Ma [d], Taomiao Wang [c], Fei Wang [c], Yonggui Sun [c], Xing'ao Li [a], Hanlin Hu [c*] and Yi Zhang [b*]

a. Jiangsu Provincial Engineering Research Center of Low-Dimensional Physics and New Energy & School of Science, Institute of Advanced Materials (IAM), Nanjing University of Posts and Telecommunications, Nanjing 210023, China
b. Institute of Molecular Plus, Tianjin University, Tianjin 300072, China.
c. Hoffmann Institute of Advanced Materials, Shenzhen Polytechnic University, 7098 Liuxian Boulevard, Shenzhen 518055, China
d. School of Mathematics and Physics, Nanjing Institute of Technology, 1 Hongjing Avenue, Nanjing 211167, China.

Email: ruiyuanhu@njupt.edu.cn; hanlinhu@szpu.edu.cn; yi_zhang@tju.edu.cn

Experimental Section

Materials: ITO glass substrates, Formamidinium Iodide (FAI), Methylammonium chloride (MACl), PbI_2 and were purchased from Advanced Election Technology Co.Ltd. Methylammonium bromide (MABr), Potassiumsulphide(K_2S) and Spiro-OMeTAD were supplied from Xi'an Polymer Light Technology Crop. Co., Ltd. Bis (trifluoromethane) sulfonimide lithium salt (Li-TFSI, 99%), 4-tert-butylpyridine (tBP, 96%) and CsI (99.99%) were supplied from Sigma-Aldrich. Tin(IV) oxide was purchased from Alfa Aesar. DMF, DMSO, IPA and acetonitrile were purchased from Aladdin. All chemicals were used as received without further treatment.

Devices Fabrications: ITO substrates were sequentially washed by detergent, deionized (DI) water, acetone, and isopropanol for 30 min through sonication method, respectively. Cleaned ITO substrates were treated with ultraviolet-ozone for 30 min, after which a SnO_2 electron transporting layer was deposited on the substrate by spin-

coating the colloidal SnO_2 in H_2O solution with 0 or 0.5 mg/mL at 4000 rpm for 30 s and annealing it for 30 min at 150 °C on a hotplate. According to the literature, a two-step sequential process was employed to fabricate the perovskite layer in the glovebox. First, 1.5 M PbI_2 precursor was dissolved in 950 ml DMF and 50 μL CsI solution (390 mg CsI in 1 mL DMSO). The above solution was then spin-coated on the SnO_2/ITO substrate at 1500 rpm for 30 s, and dried at 70 ℃ for 1 min. Thereafter, a mixture solution of FAI: MABr: MACl (90 mg: 9 mg: 9 mg in 1 mL IPA) was dropped on the PbI_2 film at 15 00 rpm for 30 s. The as-cast perovskite film was annealed at 150 °C for 15 min under 30-40% relative humidity. The spiro-OMeTAD solution was made up of 72.3 mg spiro-OMeTAD, 30 μL TBP, and 35 μL Li- TFSI solution (260 mg in 1 mL acetonitrile) in 1 mL chlorobenzene and spin-coated on above perovskite film for 30 s at 4000 rpm. Finally, a 100 nm Au electrode was deposited by thermal evaporation.

Characterization: GIWAXS measurements were conducted at the Synchrotron and Printable Electronics Laboratory at Shenzhen Polytechnic using Saxs Focus, which was equipped with a Cu X-ray source (8.05 keV, 1.54 Å) and a Pilatus3R 300K detector. The incident angle was set to 0.5°. X-ray diffraction spectra of the perovskite film were obtained by scanning angles ranging from 3 to 40° (2θ) using a Bruker D8 Advance instrument. The current-voltage characteristics of the PSC devices were evaluated using an IVS-KA6000 Enlitech sunshine simulator equipped with an AM1.5 filter under an illumination intensity of 100 $mWcm^{-2}$ and controlled by a Keithley SMU source following calibration against a standard reference cell. The J-V curves were acquired through forward scans (-0.2 to 1.2 V) followed by reverse scans (1.2 to -0.2 V). An QE-R device manufactured by Enli Technology Co. Ltd. The instrument was used to obtain the corresponding External Quantum Efficiency (EQE) spectrum under ambient conditions. Scanning electron microscopy (SEM) studies were conducted using a JSM-IT800 to observe the morphology of a perovskite thin film. EDS mapping were tested using the TM Series dedicated Energy Spectrometer (EDS). Atomic force microscope (AFM) characterizations were conducted using an Oxford Instruments MFP-3D Origin. The Edinburgh FLSP1000 spectrophotometer, equipped with a 440 nm picosecond

pulsed diode laser excitation source, was used to measure the static photoluminescence (PL) and time-resolved photoluminescence (TRPL) of the perovskite film. EIS measurements were carried out using electrochemical workstation operated from 1M Hz to 1 Hz under dark condition at 0 V. Mott−Schottky analysis of PSCs in the dark using a frequency of 1 kHz.

Elemental distribution analysis via Energy Dispersive Spectroscopy (EDS) mapping (Fig. S1, supporting information) revealed uniform dispersion of K_2S within the SnO_2 film.

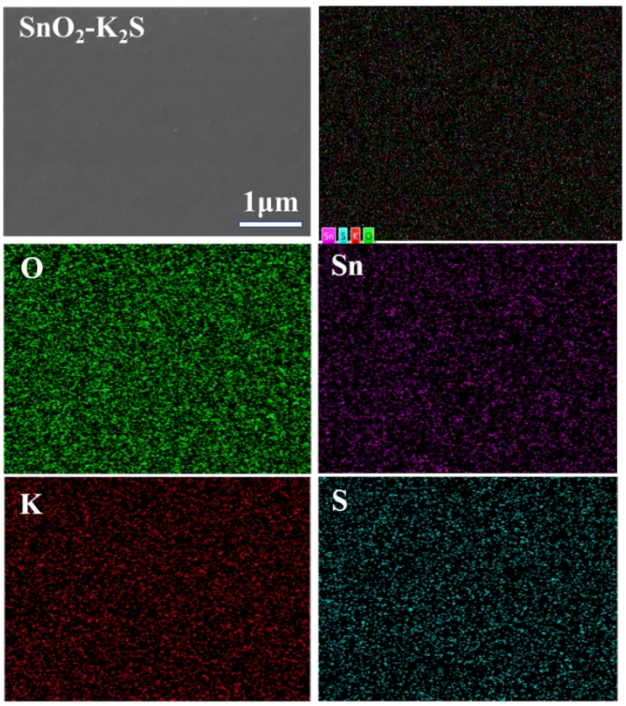

Figure S1. The EDS

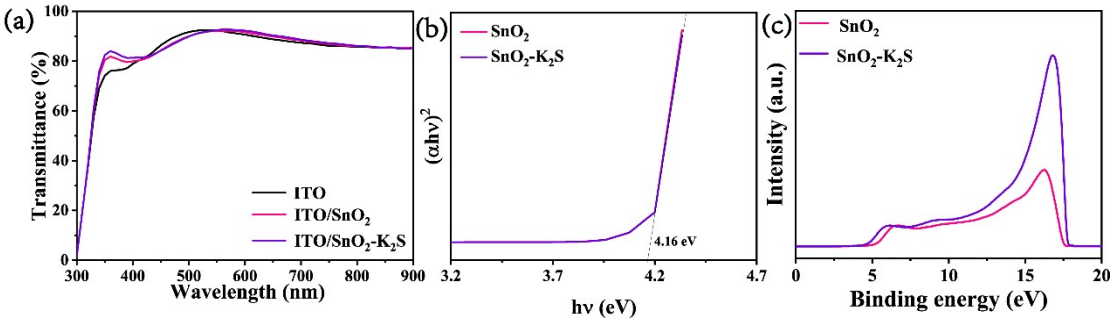

Figure S2. (a) Optical transmittance spectra of SnO_2 and SnO_2-K_2S films on ITO substrates. (b) The Tauc plots from transmittance spectra of SnO_2 and SnO_2-K_2S films. (c) The whole survey of UPS spectra of SnO_2 and SnO_2-K_2S films.

Table S1. The parameter summary from UPS test

Sample	$E_{cut\text{-}off}$(eV)	E_{onset}(eV)	WF(eV)	Eg(eV)	VB(eV)	CB(eV)
SnO_2	17.52	5.19	3.7	4.16	8.89	4.54
SnO_2-K_2S	17.74	4.91	3.48	4.16	8.39	4.23
PVK					5.59	4.03

The electrical conductivity (σ) of ETLs were evaluated by the current−voltage (I−V) curves of ITO/SnO_2(SnO_2-K_2S)/Ag structure under dark conditions. According to the formula for calculating σ:

$$\sigma = \frac{dI}{AV}$$

where d and A are nearly the same, corresponding to the thickness and active area of SnO_2 and SnO_2-K_2S.

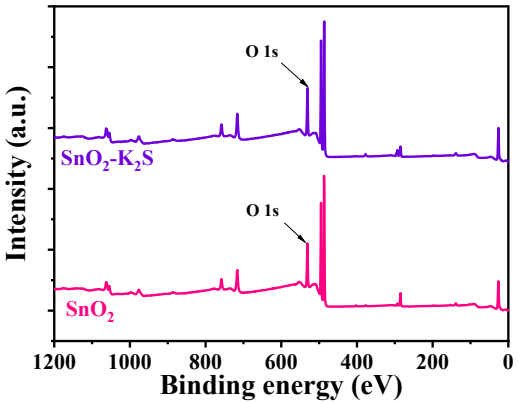

Figure S3. The whole survey XPS spectra of SnO_2 and SnO_2-K_2S film.

As the substrate for PVK film growth, the ETL is crucial to the PVK crystallization process. The morphology of the PVK film serves as a critical indicator of its crystallization quality and can be thoroughly examined using Atomic Force Microscopy (AFM) and Scanning Electron Microscopy (SEM). Compared to the SnO_2 film, significant improvements in the smoothness of the ETL are observed in SnO_2-K_2S ETL. The enhancement is clearly illustrated in the AFM images (Fig. S4a and S4b), where the surface roughness is markedly reduced. A smoother ETL can facilitate better contact with the PVK layer and minimize defects that can hinder charge transport. A

comparative analysis of the AFM morphology reveals a notable enhancement in PCK grain size deposited on the SnO_2-K_2S ETL (in Fig. S4c and S4d). Larger grains typically indicate more efficient crystal growth and fewer grain boundaries, which can enhance charge carrier mobility and reduce recombination losses. Consistent with these observations, the SEM images also demonstrate the similar trend in grain size enlargement, as evident from Fig. S4e and S4f. The SEM images provide a broader view of the film's microstructure, confirming the uniformity and quality of the crystallization process. Furthermore, pinholes as non-radiative recombination centers are clearly found in the PVK film on the SnO_2, which can impede charge transport efficiency and accelerate performance degradation in devices. In addition, the cross-sectional SEM results also reveal larger grains and a more compact structure of the PVK layer on the SnO_2-K_2S ETL, indicating improved crystallization and reduced defect density (in Fig. S4g and S4h). This enhanced crystallization can improve charge transport and the overall stability and longevity of the device. The resulting smoother surface and larger grain sizes contribute to better charge transport properties and fewer defects, ultimately leading to higher performance and more reliable optoelectronic devices.

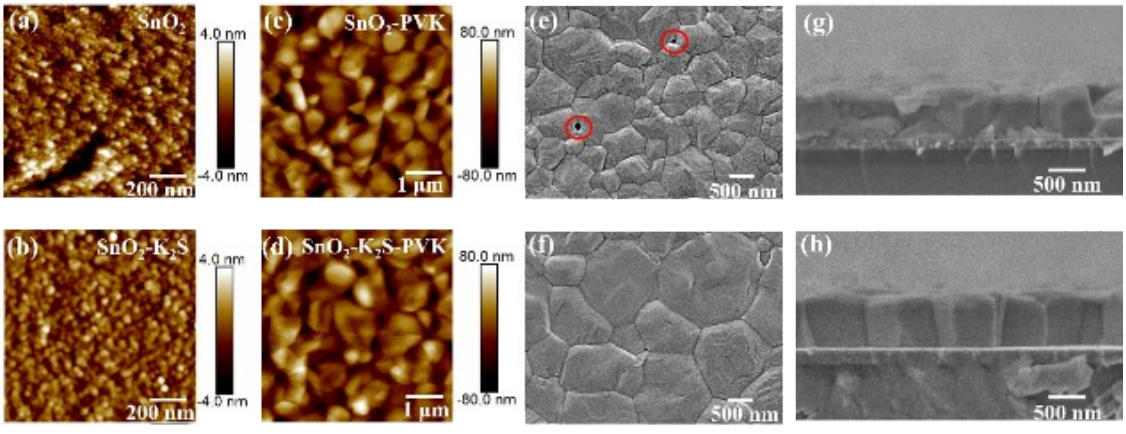

Figure S4. AFM images of (a) SnO_2, (b) SnO_2-K_2S, (c) SnO_2-PVK and (d) SnO_2-K_2S-PVK films. Top-view SEM images of (c) SnO_2-PVK and (d) SnO_2-K_2S-PVK films. Cross-section SEM images of (g) SnO_2-PVK and (h) SnO_2-K_2S-PVK films.

The fast decay (τ_1) and slow decay (τ_2) were obtained by a bi-exponential decay function:

$$y = A_1 \exp\left(-\frac{x}{\tau_1}\right) + A_2 exp(-\frac{x}{\tau_2}) \quad \text{(S1)}$$

where Ai is the amplitude and τ_i is decay time.

The average carrier lifetime was calculated by:

$$\tau_{avg} = \frac{\sum A_i \tau_i^2}{\sum A_i \tau_i} \quad \text{(S2)}$$

Table S2. Fitting parameters for TRPL spectra.

Sample	A_1	τ_1	A_2	τ_2	τ_{avg}
control	0.3412	96.34	0.6588	406.53	372.62
Target	0.4928	17.36	0.5072	334.62	319.40

n_{trap} is calculated by the threshold voltage (V_{TFL}) at the point of the Ohmic and TFL regions following the equation:

$$n_{trap} = \frac{2\varepsilon\varepsilon_0 V_{TFL}}{eL^2} \quad \text{(S3)}$$

where ε_0 is the vacuum permittivity (8.85 F/cm), ε is the relative permittivity (62.23), e is the elementary charge (1.602×10^{-19} C), and L is the thickness of the perovskite film (700 nm). The VTFL of the control device

To investigate the charge carrier transfer and recombination dynamics, electrochemical impedance spectroscopy (EIS) was conducted at a bias voltage of 0 V, as showed in Fig. S5a. The semicircle in the high-frequency region corresponds to the charge transfer resistance (Rct). The other one in low-frequency region implies to recombination resistance (Rrec). The reduced Rct and Rrec values for the target device suggested improved charge transport efficiency and reduced charge recombination. Moreover, the Mott–Schottky analysis is conducted to comprehensively evaluate carrier recombination and transport characteristics. As illustrated in Fig. S5b, the built-in potential (Vbi) of target device is 1.01 V, higher than the 0.98 V of the control device.

The increase of Vbi indicates that the incorporation of K_2S into the ETL improves carrier extraction and transport rates, thereby enhancing the *Voc*. Additionally, an analysis of dark current density provides valuable insights into charge transfer properties, as depicted in Fig. S5c. The reduced dark current density observed in the device with SnO_2-K_2S ETL suggests superior charge transfer performance, potentially leading to decreased leakage current.

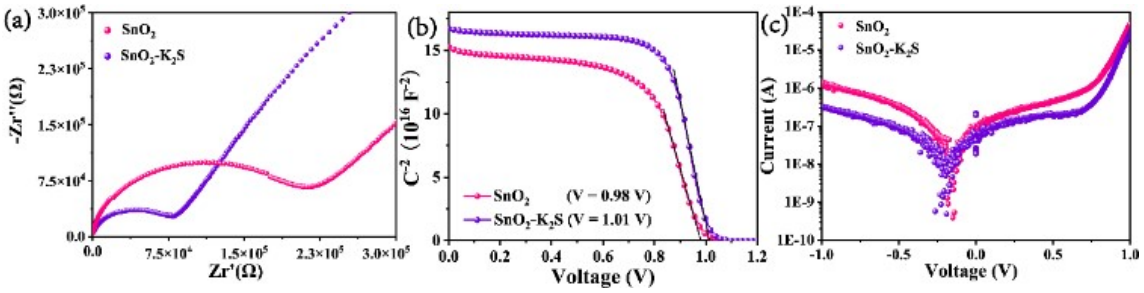

Figure S5. (a) Nyquist plots, (b) Mott–Schottky plots and (c) J–V curves under dark of devices based on SnO_2 and SnO_2-K_2S.

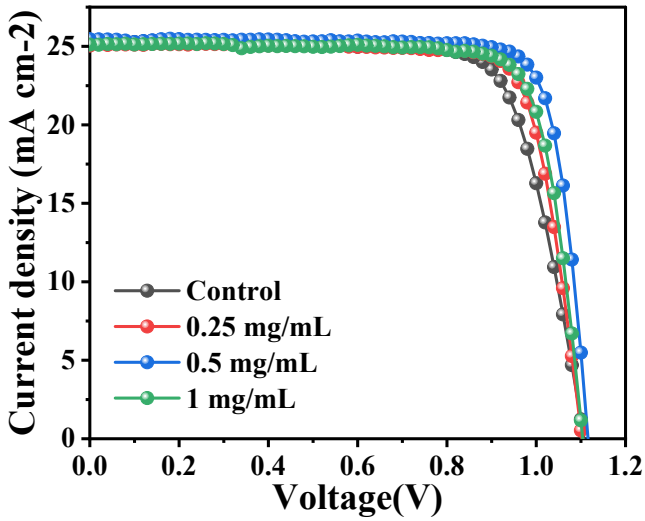

Figure S6. J-V curves of PSCs based on SnO_2-K_2S ETL with different amount of K_2S.

Table S3. The statistic parameters of the PSCs based on SnO_2-K_2S ETL with different amount of K_2S.

Sample	*J*sc (mA/cm^2)	*V*oc (V)	FF (%)	PCE (%)
Control	25.33	1.107	75.24	21.08
0.25 mg/mL	25.06	1.102	79.94	22.06

0.5 mg/mL	25.42	1.150	82.18	23.29
1 mg/mL	25.13	1.103	80.44	22.30

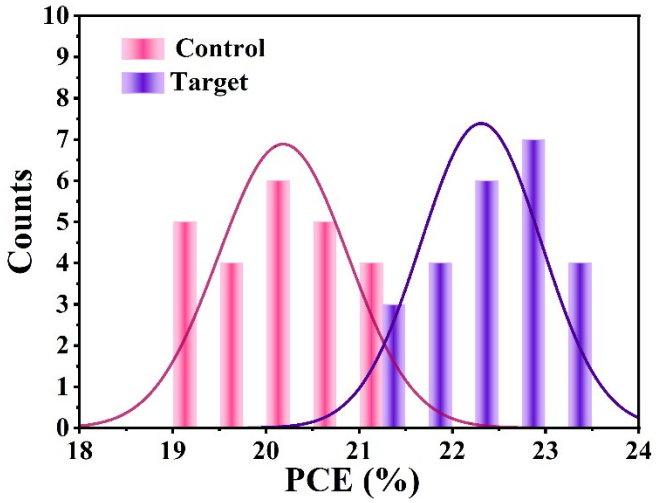

Figure S7. Diffusion statistics of control and target devices.

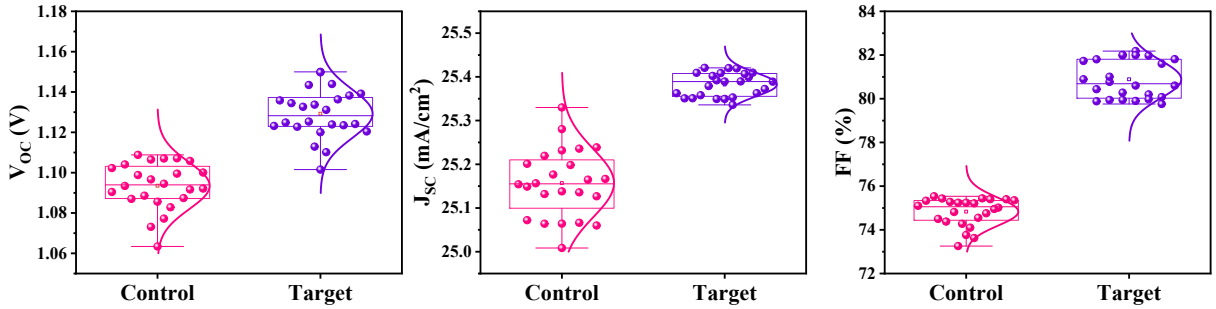

Figure S8. Statistical distribution of performance parameters for control and target devices.

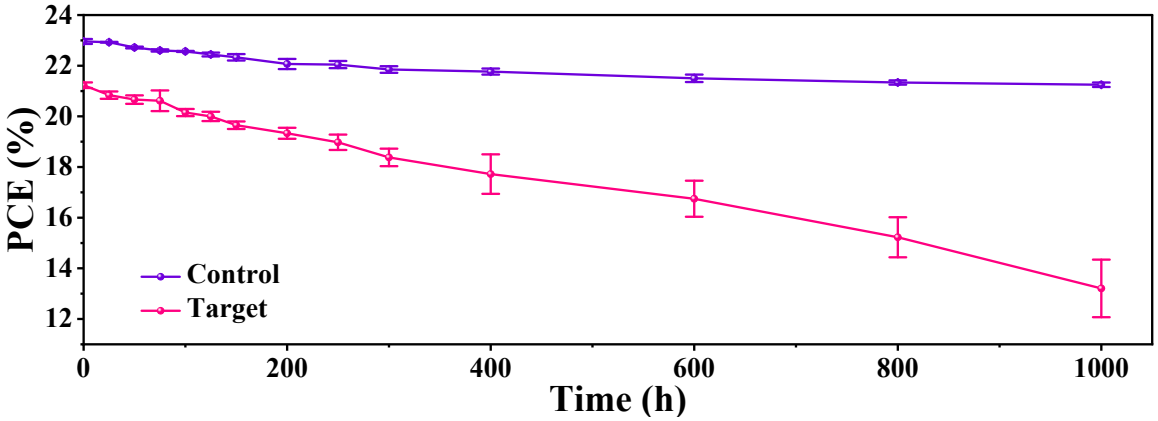

Figure S9. PCE, including standard errors, were calculated from ten control and target devices, respectively, the top and bottom stars in the PCE for the control and target devices represent the

maximum and minimum values, respectively.

Table S4. The photovoltaic parameters of champion control and target devices.

Samples	*J*sc (mA/cm^2)	*V*oc (V)	FF (%)	PCE (%)	HI
Control-Reverse	25.33	1.107	75.24	21.08	0.043
Control-Forward	25.29	1.097	72.88	20.17	
Target-Reverse	25.42	1.115	82.18	23.29	0.011
Target-Forward	25.38	1.106	81.98	23.02	